Microstructural and tribological studies of Al_2O_3/ZrO_2 nano multilayer thin films prepared by pulsed laser deposition

Balakrishnan G[1,7*], Elangovan T[2,3], Shin-Sung Yoo[3], Dae-Eun- Kim[3], Kuppusami P[4], Venkatesh Babu R[5], Sastikumar D[6], Jung il Song[7]

[1]*Department of Nanotechnology, Centre of Excellence in Patterned Multiferroics & Nanotechnology, Bharath Institute of Science and Technology, Bharath University, Chennai 600073, India*
[2]*Department of Physics, PSG College of Arts & Science, Coimbatore 641014, India*
[3]*Center for Nano-Wear, Yonsei University, Seoul-120749, South Korea*
[4]*Centre for Nanoscience and Nanotechnology, Sathyabama University, Chennai 600119, India*
[5]*Department of Mechanical Engineering, Sri Lakshmi Ammal Engineering College, Chennai 600073, India*
[6]*Department of Physics, National Institute of Technology, Tiruchirappalli 620015, India*
[7]*Department of Mechanical Engineering, Changwon National University, Changwon 641773, South Korea*

[*]Corresponding author; Tel: (91) 44-22290125; Fax: (91) 44-22290742; E-mail: balaphysics76@gmail.com

Received: 16 January 2016, Revised: 16 August 2016 and Accepted: 02 October 2016

DOI: 10.5185/amlett.2017.6434
www.vbripress.com/aml

Abstract

Nanostructured single layer aluminium oxide (Al_2O_3), single layer zirconium oxide (ZrO_2) and the (Al_2O_3/ZrO_2) nano multilayer films were deposited on Si (100) substrates at an optimized oxygen pressure of 3×10^{-2} mbar at room temperature by pulsed laser deposition. The Al_2O_3 layer was kept constant at 5 nm, while ZrO_2 layer thickness was varied from 5 nm to 20 nm. The X-ray diffraction (XRD) studies of single layer of Al_2O_3 film indicated the cubic γ-Al_2O_3, while the single layer of ZrO_2 indicated both the monoclinic and tetragonal phases. The Al_2O_3/ZrO_2 multilayer films of 5/5 nm and 5/10 nm indicated the tetragonal phase of ZrO_2 with nanocrystalline nature. The FESEM and AFM studies showed the dense and smooth morphology of the films. The pin-on disc revealed that the 5/10 nm multilayer film has low friction coefficient ~ 0.10. The wear rate of multilayers film is half of the wear rate of the single layer films and 5/10 nm multilayer film showed a reduced wear rate when it is compared to other single and multilayers. The Al_2O_3-ZrO_2 ceramics find wide applications in wear and corrosion resistance components, high temperature applications and bio-implant materials. Copyright © 2017 VBRI Press.

Keywords: Thin films, nano multilayer, microstructure, tribology, pulsed laser deposition**.**

Introduction

Formation of Al_2O_3/ZrO_2 nanolaminate structure is an important method to stabilize the high temperature phase of zirconia at room temperature. The crystallite size is controlled by reducing ZrO_2 layer thickness in the Al_2O_3/ZrO_2 nanolaminate structure [**1-3**]. Al_2O_3-ZrO_2 ceramics are extensively used as an industrial material, such as wear and corrosion resistance components, high temperature applications and bio-implant materials because of their strength, excellent chemical and thermal stability with biocompatibility [**4**]. The Al_2O_3/ZrO_2 laminar composites achieved the drastic increase in strength and fracture toughness because of various crack-shielding fact related to the presence of the layers (delamination, crack deflection etc.) [**5**]. Due to its superior performance, it is used as protective coatings against the hot corrosion. It has the potential for increasing the power and fuel efficiency of diesel and gas turbine engines [**6**]. The multilayers are also used as an encapsulation layers for large-area of organic devices [**7**]. The Al_2O_3/ZrO_2 nanolaminates are examples for transformation toughened coating [**8**]. The super plastic behaviour of ZrO_2-Al_2O_3 nanolaminate actively protects medical implant grade 316L stainless steel against perforated pitting, whereas the single layer coating of each oxide fails to protect [**9**]. The ZrO_2 and Al_2O_3 have very low solubility in steel and in each other and thus form a potential system for the formation of nanocomposites. The major failure mechanism in thermal barrier coating (TBC) is the formation of thermally grown oxide layer at the bond coat/zirconia interface. The introduction of single layer alumina or graded alumina/zirconia interlayer offers a solution to this problem by incorporating an oxygen diffusion barrier into the TBC system, thereby reducing the TGO growth rate [**10**].

The multilayer coating concept is broadly used for the protective coatings for tribological applications. It has potential for the development of new materials with tailored properties. The Nanoscale multilayer materials exhibit a wealth of interesting microstructural properties because of the increased interface area density, large strains and improved tribological properties. Tribological behaviour plays an important role in the performance of engineering applications systems such as, micro-switches, micro-gears and micro-actuators [**11**]. Wear, Fracture, creep and pitting are known as the main failure mechanisms of structural and tribological applications [**12**]. Many of these failure mechanisms are related to the tribological properties of the contacting surfaces. Therefore, tribological behaviour is a critical issue that must be properly dealt to attain the high reliability on engineering applications [**13**]. The ceramic materials have high temperature strength due to high melting point, which are compared with any other material. The high melting point can be useful in two different ways [**14**]. Primarily, high contact temperatures, which are generated at a tribological contact, depend on the friction and operating parameters and secondly high temperature machining and tribological. Due to heat dissipating problem, it is not possible to use any other material other than ceramics for tribological applications. Furthermore, due to the low density behaviour of these ceramics, it can be possible to use in tribological applications and its required lightweight components such as modulus and strength.

The Al_2O_3 and ZrO_2 toughened ceramics were used in orthopedics in the last decades. The yttria partially-stabilized tetragonal zirconia is being used in dentistry as dental implants and abutments, but also a broad range of load-bearing fixed partial dentures [**15**]. In layered structure, the presence of compressive stresses can reduce the propagation of cracks and increase all the related properties. Al_2O_3/ZrO_2 composites showed improved mechanical and tribological properties [**16**, **17**]. The reports on microstructure and tribological properties of Al_2O_3 and ZrO_2 single layer and multilayer thin films are very limited. Hence, the objective of the present study is to investigate the nanoscale effects involving different behavior in terms of microstructural and tribological properties of single layer and multilayers and develop a fundamental understanding of the microstructure and its behavior at nanoscale and this can be used for further applications as coating in dental implant coating material.

Experimental details

Material synthesis

Al_2O_3 (99.99% purity, Aldrich) and ZrO_2 (99.99% purity, Aldrich) powders were compacted into a pellets of 25 mm diameter and 3 mm thickness at a pressure of 10 MPa using a uni-axial press. The pellets were sintered at 1473 K for 6 hours and used as targets for PLD. The chamber was evacuated to 2×10^{-6} mbar using turbo molecular pump backed with rotary pump. The deposition was performed by using KrF excimer laser (Lamda Physik Model, Compex, Germany, λ=248 nm) with a pulse duration of 30 ns and energy density of about 3 J/cm^2. N-type (Phosphorous doped) Si (100) oriented substrates of dimension 10 mm×10 mm×0.5 mm were used for the film deposition. The single layer Al_2O_3 and ZrO_2 were deposited separately for 3 hrs in order to get 1 μm thickness. The four different Al_2O_3/ZrO_2 multilayers were deposited as follows:

(i) 5 nm/20 nm
(ii) 5 nm/15 nm
(iii) 5 nm/10 nm
(iv) 5 nm/5 nm

Total of 40 bilayers were deposited at an optimized oxygen partial pressure of 3×10^{-2} mbar at room temperature.

Characterizations

The deposition rates of the individual materials were determined accurately by measuring the thickness using a Dektak profilometer (DEKTAK 6M-stylus profiler by veeco, USA). The structural properties of the single and multilayer films were characterized by using X-ray diffractometer (XRD) (INEL XRG-3000 Diffractometer) attached with a curved position sensitive detector using CuKα1 (0.15406 nm) radiation. The X-ray reflectivity (XRR) studies on the multilayer films was carried out by using D8 BRUKER X-ray diffractometer with CuKα1 (1.5406 Å) radiation and with a step size of 0.001° and angular range of 0.2-8°. The intensity versus 2θ plots was converted to reflectivity versus lattice vector (*Qz*) plots. The momentum transfer (*Qz*) along the surface normal is given by equation:

$$Q_z = \frac{4\pi}{\lambda} Sin\alpha$$

where, α is the incident angle and λ_is the incident wavelength of the X-rays used. The XRR profiles were fitted using Parratt 1.5 software. Surface morphology of the films were examined by field emission scanning electron microscopy (FESEM) (TESCAN, Model: MIRA II LMH) equipped with high brightness Schottky emitter. The friction and wear properties of the coating were investigated by using a commercial reciprocating tribo-tester (CETR UMT-2). The steel ball of 1 mm diameter was used as counterpart material. The tests were conducted at room temperature, relative humidity of ~ 40 %, ball counterpart reciprocated with the velocity of 2 mm/s and load 10 mN against multilayer coating with a stroke length of 3 mm and the tests persisted for 1 h. The co-efficient of friction and number of sliding cycle were recorded automatically. The tests were carried for five times on each specimen and the average friction coefficient was calculated. The relative error for the repeated tests was not more than 5%. The wear track of single layer and multilayer coatings were observed using a scanning electron microscope (SEM; Model JSM–5610, JEOL, Japan). The chemical composition of the films was determined by using an electron probe micro analyzer (EPMA).

Results and discussion

Microstructural characterization

The sintered Al_2O_3 pellet was found to be α-alumina with a hexagonal structure (a = 4.75Å, c =12.99Å) and in agreement with JCPDS data (#46-1212). The sintered ZrO_2 pellet was found to have higher fraction of monoclinic (~75% vol.) and small fraction (25% vol.) of tetragonal phases. These two pellets were used to deposit the single and multilayer films. The XRD studies of Al_2O_3 film showed the peak at 2θ angles 45.76°, 57.0°, 67.10° corresponding to (400), (422) and (440) reflections indicating the polycrystalline cubic structure of γ-Al_2O_3 phase [**18**, **19**]. Therefore the γ-Al_2O_3 phase is obtained at room temperature due to the higher energy possessed by the ablated species and thickness of the film (~1 μm). Generally, Al_2O_3 shows the amorphous, γ, θ, δ and α phases sequentially with increasing temperature. It is noted that the nanocrystalline γ-Al_2O_3 phase is observed in the room temperature itself. The crystallite size was calculated using Scherrer formula:

$$D = \frac{K\lambda}{\beta Cos\theta}$$

where, $\beta = \sqrt{(B^2 - b^2)}$ K is Scherrer constant, λ is the wavelength of the CuKα1 (0.15406 nm) radiation, D is the crystallite size, β is full width at half maximum (FWHM) after correcting the instrumental broadening, θ is the diffraction angle, B is the observed FWHM of the film and b is the instrumental broadening for the standard Si powder. The crystallite size was found to be ~7 nm. Cibert *et al*. [**20**] prepared the single layer Al_2O_3 films by plasma enhanced chemical vapour deposition at room temperature and found that the as-deposited films were amorphous, whereas at 1073 K, the films were cubic γ-Al_2O_3. Pradhan *et al*. [**21**] prepared Al_2O_3 thin films and found that the films were amorphous in the temperature range 623-823 K, whereas crystalline Al_2O_3 phase in the temperature range 823-1023 K.

The XRD studies of ZrO_2 film showed the peaks at 2θ angles 33.76°, 34.52°, 49.65°, 55.05°, 58.96° corresponding to the reflections of m (200), t (002), t (200), m (310) and t (103), where m, t denotes the monoclinic and tetragonal phases, respectively [**22**, **23**]. Therefore, the ZrO_2 film is polycrystalline nature with monoclinic and tetragonal phases. It shows the higher intensity of tetragonal phase indicating the higher content of tetragonal phase compared to monoclinic phase. The crystallite sizes of monoclinic and tetragonal phases were calculated to be 23 nm and 27 nm, respectively. Misun Chun *et al.* [**24**] deposited ZrO_2 films on Si (100) in the substrate temperature range 300-623 K and found that all the films contain only monoclinic phase. Balakrishnan *et al.* [**23**] deposited ZrO_2 thin films at different substrate temperature by pulsed laser deposition and found both monoclinic and tetragonal phases.

Fig. 1 shows the XRD pattern of Al_2O_3/ZrO_2 multilayer films. The 5/20 nm and 5/15 nm multilayer films showed broad peak ~ 31.2°, indicating the overlap of monoclinic and tetragonal phases with nanocrystalline nature.

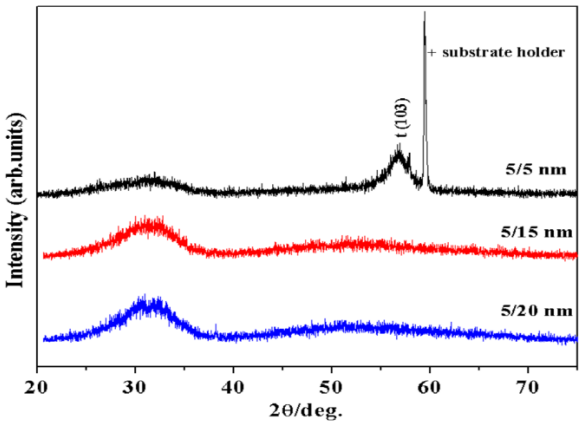

Fig. 1. XRD pattern of the Al_2O_3/ZrO_2 multilayer films.

The 5/10 nm and 5/5 nm multilayer films showed two prominent peaks at 2θ values of 30.6°, 56.7° indicating (101) and (103) reflections of tetragonal ZrO_2 with nanocrystalline nature. The crystallite sizes was calculated for 5/10 nm and 5/5 nm films and found to be 6-10 nm and 4-8 nm, respectively. Al_2O_3 was amorphous in all the multilayer films. Al_2O_3 is a template for the ZrO_2 layer and stabilization of metastable phase of ZrO_2. The layer thickness is the very important parameter for stabilization of tetragonal ZrO_2. When the layers are very thin, the interfacial and surface energies dominate, which could promote the formation of a metastable phase with low interfacial energy. In the Al_2O_3/ZrO_2 nanolaminates, Al_2O_3 has negligible solubility within ZrO_2 and it forms a rigid matrix around the ZrO_2 crystals, which provides a local compressive stress, and hinders the phase transformation. Also, Al_2O_3 has almost twice the elastic constant (390 GPa) compared to that of ZrO_2 (207 GPa). The high elastic constant of alumina provides structural stability for the tetragonal phase of ZrO_2 and inhibits the growth of monoclinic.

Teixeira *et al.* [**25**] deposited ZrO_2/Al_2O_3 multilayers by DC reactive magnetron sputtering and found that the tetragonal phase content were increased with decreasing ZrO_2 layer thickness. Gao *et al.* [**1**] prepared Al_2O_3/ZrO_2 multilayers by DC magnetron sputtering with ZrO_2 layer thickness in the range ~ 8-20 nm and found that the multilayers were exhibited excellent thermal stability after annealing. Aita *et al.* [**26**] deposited nanolaminate films of ZrO_2-Al_2O_3, ZrO_2-Y_2O_3 and ZrO_2-TiO_2. The results indicated that the structure of the ZrO_2 films strongly depend on the thickness of ZrO_2 film in the Al_2O_3/ZrO_2 multilayers. Balakrishnan *et al.* [**27-29**] worked on Al_2O_3/ZrO_2 multilayers for the stabilization of ZrO_2 at room temperature and its microstructure and optical properties. Garvie *et al.* [**30**, **31**] observed t-ZrO_2 at room temperature, when the particle size of the tetragonal phase is smaller than 30 nm. Tetragonal ZrO_2 has lower free energy compared to monoclinic ZrO_2 for the same crystallite sizes. Since alumina and zirconia exhibit limited solid solubility at equilibrium, the preparation of

such metastable mixtures are necessarily involves in a nonequilibrium process. The film structures and phase stabilities depend upon ZrO_2 layer thickness. For most engineering applications, ZrO_2 is stabilised in its tetragonal structure, thus avoiding the phase transformation from tetragonal to monoclinic at about 1233-1453 K [**32**].

Zhitomirsky *et al.* [**33**] deposited the nanomultilayered Zr–O/Al–O coatings having a bi-layer period of 6–7 nm and total coating thickness of 1.0–1.2 μm by using a cathodic vacuum arc plasma process on Si substrates. Transmission electron microscopy studies revealed the nano-multilayered structure Zr–O/Al–O coatings with distinguished alternating layers. Thermal barrier coatings (TBCs) with nano-multilayer structure were investigated by thermal shock test. The change of insulation effect during thermal shock test was studied. Microstructure and electrical properties of TBCs were studied by SEM and Impedance Spectroscopy, respectively. With thermal shock, the insulation effect decreased due to the further growth of microcracks in top coat of TBC [**34**]. ZrO_2/Al_2O_3 micro-laminated coatings were deposited on stainless steel by electrolytic deposition. The as-deposited ZrO_2/Al_2O_3 coatings were characterized by field emission scanning electron microscopy (FESEM) and XRD. The results indicated that the coatings had alternate six layers of ZrO_2 and Al_2O_3 with nano/micro-structures. The phase composition of the coating was t-ZrO_2, α-Al_2O_3 and θ-Al_2O_3. High temperature cyclic oxidation test at 900 °C in air for 200 h was adopted to investigate the oxidation resistance of the coatings on stainless steel. The results revealed that ZrO_2/Al_2O_3 micro-laminated coatings improved the oxidation and spallation resistance of stainless steel substrate significantly [**35**].

XRR is a powerful technique for investigating surfaces and multilayers. XRR study was performed on multilayer films to study the formation of multilayers, individual layer thickness, bilayers thickness and surface roughness. XRR profile was obtained by plotting the scattered X-ray intensity against the angle of incidence θ. The intensity and peak position of the reflectivity curves is related with the roughness and thickness of the layers in the multilayer films, whereas the Bragg peak gives the bi-layers periodicity [**29**].

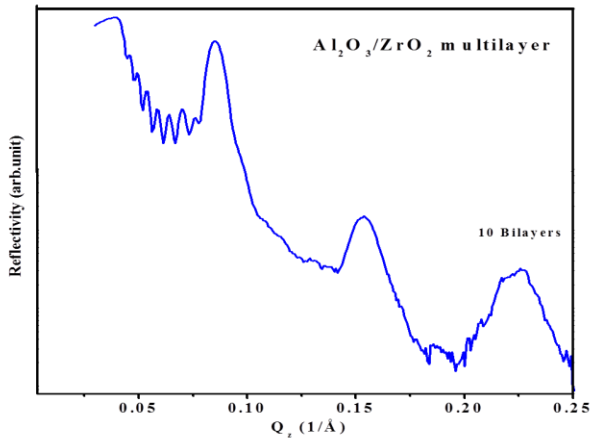

Fig. 2. XRR pattern of the 5/10 nm Al_2O_3/ZrO_2 multilayer film.

Fig. 2 shows the X-ray reflectivity studies of the typical Al_2O_3/ZrO_2 (5/10 nm) multilayer film with 10 bilayers on Si (100). It shows the Kiessig fringes (8 fringes) and sharp Bragg peaks, indicating the well-defined formation of individual layers and bilayer periodicity in the multilayer films. FESEM was used to observe the surface morphology of as-deposited Al_2O_3/ZrO_2 multilayers. **Fig. 3** shows the surface morphology of the typical $(5/10\ nm)_{40}$ and $(5/5\ nm)_{40}$ multilayer films are dense and uniform. The multilayer films were showed the uniform crystallites distribution with smooth morphology. The energy dispersive analysis of X-ray (EDAX) shows the presence of the Al_2O_3 and ZrO_2 with O_2/Al and O_2/Zr of 1.56 and 2.08, respectively. It indicates the stoichiometry of both Al_2O_3 and ZrO_2.

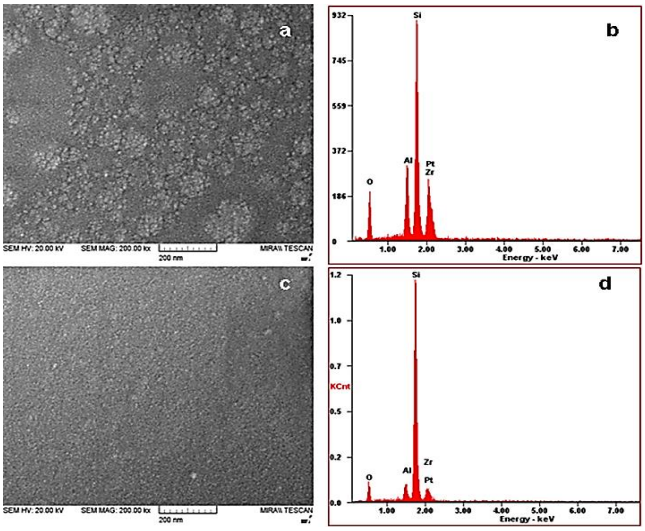

Fig. 3. FESEM images show the surface morphology of the as-deposited (a) 5/10 nm and (c) 5/5 nm multilayer films and (b) EDAX of 5/10 nm and (d) 5/5 nm films.

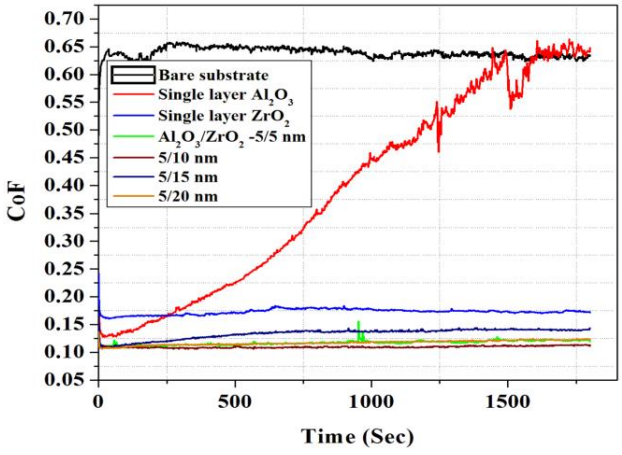

Fig. 4. Coefficient of friction of single and multilayers coatings.

Tribological Properties

Fig. 4 shows the friction behaviour of single layer Al_2O_3, ZrO_2 and Al_2O_3/ZrO_2 multilayers films in interaction with stainless steel ball at constant load of 10 mN. The results indicated the unstable frictional behaviour for single layer

coating as a function of time, contrary, the multilayer coatings are showed the steady-state behaviour. The friction coefficient value of bare substrate and single layer coating was ~0.60. It was interesting to note that the friction coefficient of different Al_2O_3/ZrO_2 multilayers coating was ~ 0.10-0.18. Among the different multilayer of Al_2O_3/ZrO_2 coatings, the 5/10 nm coating showed very low value of friction coefficient ~ 0.10. Friction and wear are important analysis for coatings. The standard wear equation was proposed by Archard [**36**].

$$Wearrate = \frac{V}{W \times L}$$

The wear rate of the stainless steel ball specimens was estimated from the above equation. The amount of wear was calculated from the 2-D cross-sectional profile of the wear track obtained by 3D Profile meter. The 2-D profiles were measured at five different places on wear track region and an average wear depth was obtained. The wear volume was estimated from the cross-sectional area of the wear track below the horizontal line of the specimen surface. **Fig. 5** illustrates the SEM images of the wear track on bare substrate and coatings such as, single layer Al_2O_3, ZrO_2, and Al_2O_3/ZrO_2 multilayers of 5/5 nm, 5/10 nm and 5/20 nm coatings against SS ball at 10 mN. The worn surface of bare substrate showed plastic deformation due to shear force.

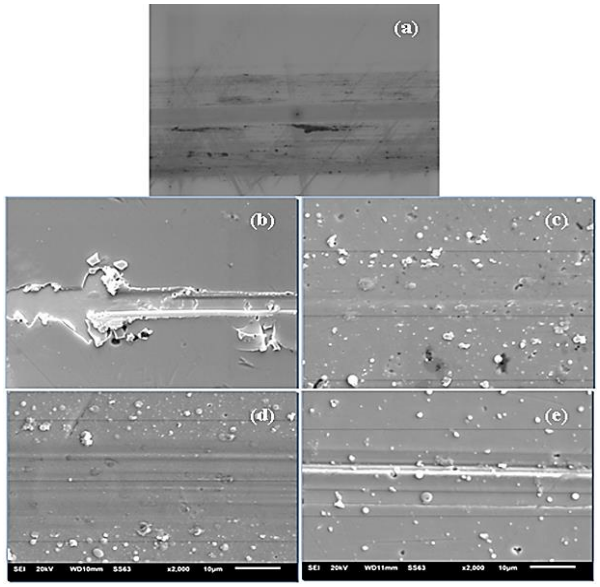

Fig. 5. SEM image shows the wear track of single and multilayer coatings (a) bare substrate (b) Al_2O_3 coating (c) 5/5 nm (d) 5/10 nm and (e) 5/20 nm coatings.

Fig. 5b shows the single layer Al_2O_3 coating worn surface, where heavy crack was observed. The 5/5 nm multilayer coating worn surface show smooth behaviour with large particles **(Fig. 5c)**. **Fig. 5d** shows that worn surface of 5/10 nm multilayer coating and confirmed the smooth wear track without any large particles were compared to any other worn surface. The results indicated that the 5/10 nm multilayer coating had excellent wear resistance due to the strong interaction bond between substrate and coating. It may be due to the minimising interfacial shear stress and distributing the load over a larger area when the applied load on the multilayer coating was compared to single layer coating [**37**].

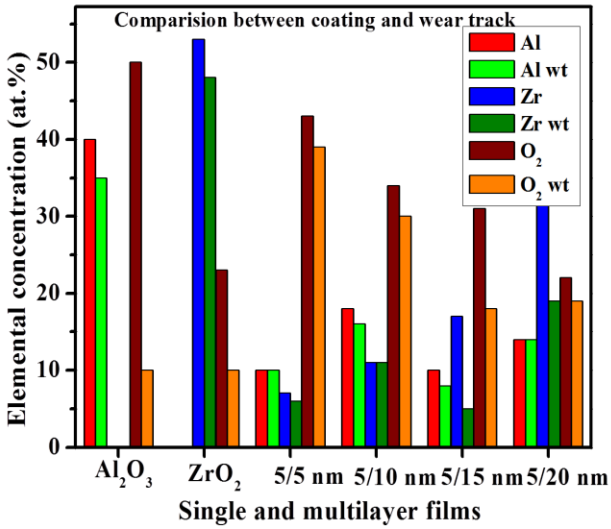

Fig. 6. EDAX analysis comparison between coatings and wear track.

In order to confirm these results, the EDAX analysis was carried out to each of these specimens and composition present in the coatings and wear tracks is shown in **Fig. 6**. It does not show much change in the elemental composition present in the coatings and on the wear tracks before and after the friction tests. The results clearly suggest that the multilayer Al_2O_3/ZrO_2 coatings of 5/5 nm, 5/10 nm, 5/15 nm and 5/20 nm does not show any changes in elemental composition between coatings and wear tracks. It is interesting to note that these multilayer coatings exhibit completely different wear mechanism was compared to single layer coatings. The enhanced wear resistance of present multilayer coatings can be attributed to many factors such as surface morphology, structural behavior, internal stress and decreases in the coefficient of friction. In the case of single layer coating lower internal stress could be expected, on contrary when coupling two different materials in a multilayer configuration, residual stresses can arise mainly due to the different thermal expansion of the materials. It resulted in multilayer coating had good wear resistance properties than single layer coating. Multilayers individual layers resulted high fraction of interface volume than single layer coating, it causes allowing strength and toughness in the coatings.

Fig. 7(a) shows the wear depth of single and multilayer coatings. For the single layer coating, the wear depth value was ~ 4 μm. With multilayer coating, the wear depth value decreased to ~ 0.64 μm. **Fig. 7b** shows the calculated wear rate of the single layer and multilayer coatings. For Al_2O_3 and ZrO_2 coatings, the wear rate values were ~5×10^{-4} mm^3/Nm. The wear rate (0.5×10^{-4} mm^3/Nm) was reduced to 50% for 5/5 nm and 5/10 nm multilayer coatings. Furthermore, the 5/15 nm

and 5/20 nm multilayers showed the wear rate of ~ 1.40×10^{-4} mm^3/Nm. Among the four different multilayer coatings, the wear rate of 5/10 nm multilayer is very low. The changes in the wear behaviour of Al_2O_3/ZrO_2 coatings with the sliding body can be explained with the microstructure and composition of the of wear tracks. Al_2O_3 thin films were deposited on Si (100) and Ni-20Cr substrates by combustion chemical vapor deposition. The film showed the friction coefficient of ~0.7 and reached a minimum value of ~0.5 at higher sliding distances. The wear rate of Al_2O_3 film was $10.1\pm1.0\times10^{-9}$ mm^3/Nm for the film deposited at 1173 K [**38-41**].

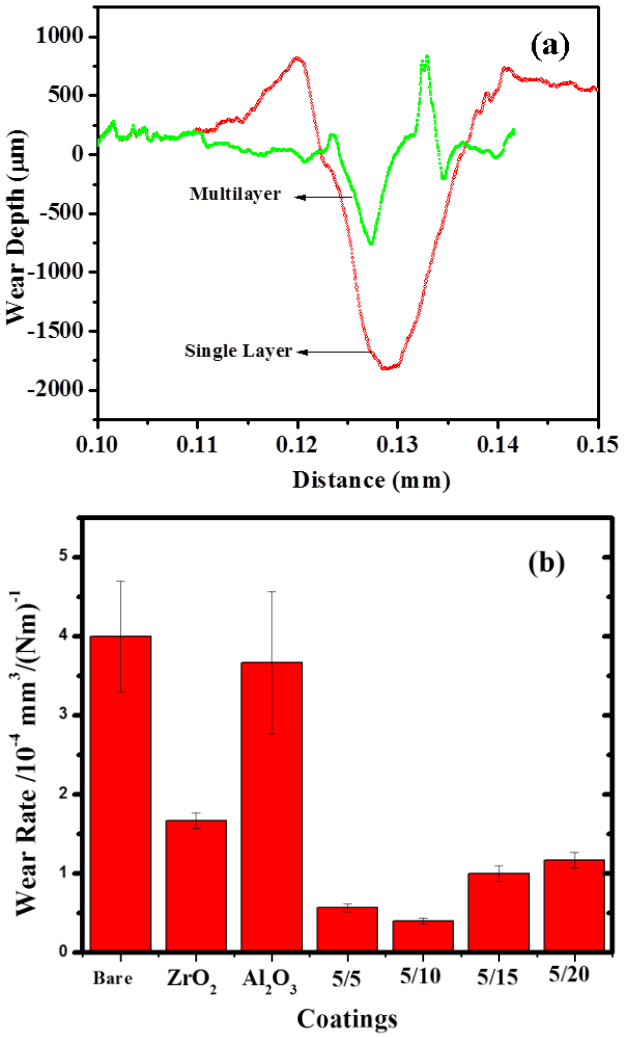

Fig. 7. (a) Typical surface profiles of the wear track of the single layer and multilayer coating (b) Variation of the wear rates of the single layer and multilayer coatings.

The friction and wear properties of the nanostructured and traditional ZrO_2 coatings against stainless steel were investigated. It was noted that the friction coefficients of nanostructured ZrO_2 coating was ~1.5 compared to the traditional ZrO_2 coating friction coefficient of 1.75. It was also found that the nanostructured ZrO_2 coating showed better wear resistance than the traditional ZrO_2 coating. The wear rates of the nanostructured ZrO_2 coatings are about two-fifths of traditional ZrO_2 coatings. The improved wear resistance of the nanostructured ZrO_2 coatings is attributed to the optimization of microstructure and enhancement of mechanical properties, which improved the ability of plastic deformation of materials [**42**, **43**]. The present work gives the developments in tribological properties are based on the multilayer coating concept. Theoretical model for the design of laminated structures and preparation for Al_2O_3-ZrO_2 layered structures was suggested by Portu *et al*. [**44**]. Al_2O_3/TiO_2 multilayer coating showed higher wear resistance over monolithic Al_2O_3 and TiO_2 (45]. The nano multilayers such as TiN/Ti, CrN/Cr, TiN/SiN*x*, TiN/CrN and TaN/NbN are reported that they have better wear resistance than their corresponding single layer films [**46-49**] and also such results was not found in a number of nano multilayers [**50**]. Ahmed A. Madfa and Xiao-Guang Yue review the current status of the functionally graded dental prostheses based on Alumina and zirconia-based ceramics to improve the performance compared to traditional dental prostheses. It opens a new path for recent researches for further development of new ceramic dental restorations [**51**]. The wear studies were indicated both the friction coefficients and wear rates increased when decreasing bilayer thickness. It is also noticed that the multilayer coatings showed excellent wear resistance, when it is compared to monolayer coating. The wear property is dependent on the crystalline nature, surface roughness and crystallite size of the films. The nanometer scale wear depth of the multilayer film changes with the layer period. The tribological behaviour has been related to the presence of compressive residual stress at the surface [**52**]. In addition to the properties of individual layer materials, the grain boundaries and interfaces play an important role for overall properties in the nanoscale coatings. It was already established that the optimum properties and performance could be achieved at specific interface volume. All the properties were not obtained their optimum levels at the same interface volume/same number of layers [**53**, **54**]. This work on nanoscale multilayer coatings showed an outstanding properties and new suggestions for the development of advanced coatings.

Conclusion

The single layer Al_2O_3, ZrO_2 and multilayer Al_2O_3/ZrO_2 films were deposited on Si (100) substrates at room temperature by PLD. The Al_2O_3 layer thickness was kept constant at 5 nm, while the ZrO_2 layer thickness was varied from 5 to 20 nm. The XRD studies of single layer Al_2O_3 indicated the cubic γ-Al_2O_3 phase, while the single layer ZrO_2 showed both monoclinic and tetragonal phases. The Al_2O_3/ZrO_2 multilayer films of 5/5 nm and 5/10 nm showed the tetragonal phase at room temperature and hence the high temperature tetragonal ZrO_2 phase was stabilized at room temperature through nano multilayer approach. Al_2O_3 was amorphous in all the Al_2O_3/ZrO_2 multilayers films. The XRR studies confirmed the formation of multilayers with uniform periodicity. The FESEM shows the uniform, dense and smooth

morphology of the films. The multilayers films showed low friction coefficients of ~0.1 and higher wear resistance with compared to the single layer films. The Al_2O_3/ZrO_2 of 5/10 nm film showed high wear resistance, when it is compared to other single and multilayer films.

Acknowledgments

This work was supported by the National Research Foundation of Korea (NRF) grant funded by the Government of the Republic of Korea (Ministry of Science, ICT and Future Planning (MSIP)) (No. 2013R1A2A2A01017108 and 2011-0030058).

Author's contributions

Conceived the plan: PK, DS; Performed the expeirments: GB; Data analysis: TE, SSY, DEK; Wrote the paper: RV, JI Song. All authors read and approved the final manuscript. Authors have no competing financial interests.

References

1. Gao, P., Meng, L. J, Dos Santos, M. P, Teixeira. V., Andritschky, M.; *Vacuum*, **2002**, 64, 267. **DOI:** 10.1016/S0042-207X (01) 00311-6.
2. Aita, C. R.; *Surf Coat Technol.*, **2004**, 188-189, 179. **DOI:** 10.1186/1556-276X-8-82.
3. Teixeira, V., Monteiro, J., Duarte, J., Portinha, A.;*Vacuum*, **2002**, 67, 477. **DOI:** 10.1016/S0042-207X (02) 00235-X.
4. Ashutosh Tiwari, Atul Tiwari (Eds), In the Nanomaterials in Drug Delivery, Imaging, and Tissue Engineering, John Wiley & Sons, USA, **2013**.
5. Oeschner, M., Hillman, C., Lange, F. F.; *J. Am. Ceram. Soc.*, **1996**, 79, 1834. **DOI:** 10.1111/j.1151-2916.1996.tb08003.x.
6. Qadri, S. B., Horwitz, J. S., Chrisey, D. B., Donovan, E. P., Skelton, E. F.; *Surf. Coat. Technol.*, **1996,** 86-87, 149. **DOI:** 10.1016/S0257-8972(96)03003-4.
7. Meyer, J., Görrn, P., Bertram, F., Hamwi, S., Winkler, T., Johannes, H.H., Weimann, T., Hinze, P., Riedl, T. and Kowalsky, W.; *Adv. Mater.*, **2009**, 21, 1845. **DOI:** 10.1002/adma.200803440.
8. Songjun Li, Yi Ge, Ashutosh Tiwari, Shunsheng Cao (Eds), In the A Temperature-Responsive Nanoreactor, WILEY-VCH Verlag, USA, **2010**.
9. Gaertner, W. F., Hoppe, E. E., Omari, M. A., Sorbello, R. S., Aita, C. R.; *J. Vac. Sci. Technol. A*, **2004**, 22, 272. **DOI:** 10.1116/1.1642650.
10. Leushake, U., Krell, T., Schulz, U., Peters, M., Kaysser, W. A., Rabin, B. H.; *Surf. Coat. Technol.*, **1997**, 94-95, 131. **DOI:** 10.1186/1556-276X-8-82.
11. Kim, H. J., Kim, D. E.; *Int. J. Prec. Eng. Manuf.*, **2009**, 10, 141. **DOI:** 10.1007/s12541-009-0039-7.
12. Sung, I. H., Lee, H. S., Kim, D. E.; *Wear*, **2003**, 254, 1019. **DOI:** 10.1016/S0043-1648(03)00308-9.
13. Kim, D.W., Lee, K.Y., Jun, Y., Lee, S., Park, C. K., *Int. J. Prec. Eng. Man.*, ***2011***, 12, 1111. **DOI:** 10.1007/s11249-012-0008-7.
14. Bikramjit B., Mitjan K.; *John Wiley & Sons*, **2011**.
15. Piconi, C., Condò, S. and Kosmaˇc, T.; *Oxford*, **2014**, 219. **DOI:** 10.1016/B978-0-12-394619-5.00011-0.
16. Bermejo, R., Sánchez-Herencia, A. J., Llanes, L., Baudín, C.; *Acta Mater.*, **2007**, 55, 4891. **DOI:** 10.1016/j.actamat.2007.05.005.
17. Parente, P., Ortega, Y., Savoini, B., Monge, M. A., Tucci, A., Esposito, L., Sa´nchez-Herencia, A. J.; *Acta Mater.*, **2010**, 58, 3014. **DOI:** 10.1016/j.actamat.2010.01.033.
18. Balakrishnan, G., Sundari S. T., Ramaseshan, R., Thirumurugesan, R., Mohandas, E., Sastikumar, D., Kuppusami, P., Kim, T. G., Song, J. I. ; *Ceram. Int.*, **2013**, 39, 9017. **DOI:** 10.1016/j.ceramint.2013.04.104
19. Balakrishnan, G., Kuppusami, P., Sundari S. T., Thirumurugesan, R., Ganesan, V., Mohandas, E., Sastikumar, D.; *Thin Solid Films*, **2010**, 518, 3898. **DOI:** 10.1016/j.tsf.2009.12.001.
20. Cibert, C., Hidalgo, H., Champeaux, C., Tristant, P., Tixier, C., Desmaison, J., Catherinot, A.; *Thin Solid Films*, **2008**, 516, 1290. **DOI:** 10.1016/j.tsf.2007.05.064.
21. Pradhan, S. K, Philip, J. R., Yeonkyu, K.; *Surf. Coat. Technol.*, **2004**, 176, 382. **DOI:** 10.1016/j.jnoncrysol.2012.12.013.
22. Balakrishnan, G., Sairam, T. N., Kuppusami, P., Thiumurugesan, R., Mohandas, E., Ganesan, V., Sastikumar, D.; *Appl. Surf. Sci.*, **2011**, 257, 8506. **DOI:** 10.1016/j.apsusc.2011.05.003.
23. Balakrishnan, G., Thanigaiarul, K., Sudhakara, P., Song, J. I; *Appl Phys A-Mater.*, **2013**, 110, 427. **DOI:** 10.1007/s00339-012-7232-8.
24. Chun, M., Moon, M. J., Park, J., Kang, Y. C.; *B. Kor. Chem. Soc.*, **2009**, 30, 2729. **DOI:** 10.5012/bkcs.2009.30.11.2729.
25. Teixeira, V., Andritschky, M., Fischer, W., Buchkremer, H. P., Stover, D.; *Surf. Coat. Technol.*, **1999**, 120-121, 103. **DOI:** 10.1016/S0257-8972(99)00341-2.
26. Aita, C. R., Wiggins, M. D., Whig, R., Scanian, C. M., Josifovska, M. G.; *J. Appl. Phys.*, **1996**, 79, 1176. **DOI:** 10.1063/1.360902.
27. Balakrishnan, G., Kuppusami, P., Murugesan, S., Ghosh, C., Divakar, R., Mohandas, E., Sastikumar, D.; *Chem. Phy.*, **2012**, 133, 299. **DOI:** 10.1016/j.matchemphys.2012.01.027.
28. Balakrishnan, G., Kuppusami, P., Sastikumar, D., *Nanoscale Res. Lett.*, **2013**, 8, 1. **DOI:** 10.1186/1556-276X-8-82.
29. Balakrishnan, G.., Sairam, T. N., Reddy, V. R., Kuppusami, P., Song, J. I.; *Mater. Chem. Phy.*, **2013**, 140, 60. **DOI:** 10.1016/j.matchemphys.2013.02.053.
30. Garvie, R. C.; *J. Phys. Chem.*, **1978**, 82, 218. **DOI:** 10.1021/j100491a016.
31. Garvie, R. C., Chan, S. K.; *Physica B*, **1988**, 150, 203. **DOI:** 10.1016/0378-4363(88)90123-4.
32. Lange, F. F.; *J. Mater. Sci.*, **1982**, 17, 225. **DOI:** 10.1007/BF00809057.
33. Zhitomirsky V.N., Kim, S. K., Burstein, L., Boxman, R. L.; *Appl. Surf. Sci.*, **2010**, 256, 6246. **DOI:** 10.1016/j.apsusc.2010.03.149.
34. Zhang, C., Zhou, C., Peng, H., Gong, S., Xu, H.; *Surf. Coat. Technol.*, **2007**, 201, 6340. **DOI:** 10.1016/j.surfcoat.2006.11.042.
35. Junguo, G., Yedong, H., Deren, W.; *Mat. Chem. Phys.*, **2010**, 123, 731. **DOI:** 10.1016/j.matchemphys.2010.05.047.
36. Archard, J. F.; *J. Appl. Phys.*, **1953**, 24, 981-988. **DOI:** 10.1063/1.1721448.
37. Penkov, O.V., Bugayev, Y. A., Zhuravel, I., Kondratenko, V. V., Amanov, A., Kim, D. E.; *Tribol. Lett.*, **2012**, 48, 123. **DOI:** 10.1007/s11249-012-0008-7.
38. Zhang, W., Liu, W., Xue, Q.; *Mater. Res. Bull.*, **2001**, 36, 1903. **DOI:** 10.1016/S0025-5408(01)00673-0.
39. Ashutosh Tiwari, Anthony PF Turner (Eds), Biosensors Nanotechnology, John Wiley & Sons, USA, .
40. Bromark, M., Larsson, M., Hedenqvist, P., Hogmark, S.; *Surf. Coat. Technol.*, **1997**, 90, 217. **DOI:** 10.1016/S0257-8972(96)03141-6.
41. Dhonge, B.P., Mathews, T., Kumar, N., Ajikumar, P.K., Manna, I., Dash, S. and Tyagi, A.K.; *Surf. Coat. Technol.*, **2012**, 206, 4574. **DOI:** 10.1016/j.surfcoat.2012.05.011.
42. Liu, J. F., Nistorica, C., Gory, I., Skidmore, G., Mantiziba, F. M., Gnade, B.E.; *Thin Solid Films*, 2005, 492, 6. **DOI:** 10.1016/j.tsf.2005.06.014.
43. Chen, H., Zhang, Y., Ding, C.; *Wear*, **2002**, 253, 885. **DOI:** 10.1016/S0043-1648(02)00221-1.

44. De Portu, G., Micele, L., Pezzotti, G.; *Compos. Part B-Eng.*, **2006**, 37, 556.
DOI: 10.1016/j.compositesb.2006.02.018.
45. Freyman, C.A., Chung, Y.W.; *Surf. Coat. Technol.*, **2008**, 202, 4702.
DOI: 10.1016/j.surfcoat.2008.04.053.
46. Zhang Z. G, Rapaud O., Allain N., Mercs D., Baraket M., Dong C., Coddet C.; *Appl. Surf. Sci.*, **2009**, 255, 4020.
DOI: 10.1016/j.apsusc.2008.10.075.
47. Boutos, T.V., Sanjines, R. and Karimi, A.; *Surf. Coat. Technol.;* **2004**, 188-189, 409.
DOI: 10.1016/j.surfcoat.2004.08.039.
48. Yao S. H, Su Y. L., Kao W. H, Liu T. H.; *Tribol. Int.*, **2006**, 39, 332.
DOI: 10.1016/j.triboint.2005.02.015.
49. Yu, X., Lai, Q., Li, G., Junhuaxu, M. G.; *J. Mater. Sci. Lett.*, **2002**, 21, 1671.
DOI: 10.1023/A:1020872625561.
50. Shinn, M., Hultman, L., Barnett, S. A.; *J. Mater. Res.*, **1992**, 7, 901.
DOI: 10.1557/JMR.1992.0901.
51. Madfa, A. A., Yue, X. G.; *Jan Dent. Sci. Rev.*, **2016**, 52, 2.
DOI: 10.1016/j.jdsr.2015.07.001.
52. Chu, K., Shen, Y. G.; *Wear* **2008**, 265, 516.
DOI: 10.1016/j.wear.2007.11.021.
53. Stueber, M., Holleck, H., Leiste, H., Seemann, K, Ulrich, S, Ziebert, C.; *J. Alloy. Compd*., **2009**, 483, 321.
DOI: 10.1016/j.jallcom.2008.08.133.
54. Ghosh, C., Ramachandran, D., Balakrishnan, G., Kuppusami, P. and Mohandas, E.; *Bull. Mater. Sci.*, **2015**, 38, 1.
DOI: 10.1007/s12034-014-0838-z.